IOP Publishing Journal of Physics: Condensed Matter
J. Phys.: Condens. Matter **32** (2020) 255701 (9pp) https://doi.org/10.1088/1361-648X/ab7ada

Interaction between Mo and intrinsic or extrinsic defects of Mo doped $LiNbO_3$ from first-principles calculations

Weiwei Wang, Hongde Liu[1], Dahuai Zheng, Yongfa Kong[1], Lixin Zhang and Jingjun Xu

MOE Key Laboratory of Weak-Light Nonlinear Photonics & School of Physics and TEDA Institute of Applied Physics, Nankai University, Tianjin 300071, People's Republic of China

E-mail: liuhd97@nankai.edu.cn and kongyf@nankai.edu.cn

Received 16 December 2019, revised 10 February 2020
Accepted for publication 27 February 2020
Published 27 March 2020

Abstract

Lithium niobate ($LiNbO_3$, LN) plays an important role in holographic storage, and molybdenum doped $LiNbO_3$ (LN:Mo) is an excellent candidate for holographic data storage. In this paper, the basic features of Mo doped $LiNbO_3$, such as the site preference, electronic structure, and the lattice distortions have been explored from first-principles calculations. Mo substituting Nb with its highest charge state +6 is found to be the most stable point defect form. The energy levels formed by Mo with different charge states are distributed in the band gap, which are responsible for the absorption in the visible region. The transition of Mo in different charge states implies molybdenum can serve as a photorefractive center in LN:Mo. In addition, the interactions between Mo and intrinsic or extrinsic point defects are also investigated in this work. Intrinsic defects V_{Li}^{-} could cause the movement of the Mo_{Nb}^{+} energy levels. The exploration of Mo, Mg co-doped $LiNbO_3$ reveals that although Mg ion could not shift the energy level of Mo, it can change the distribution of electrons in Mo and Mg co-doped LN (LN:Mo,Mg) which help with the photorefractive phenomenon.

Keywords: lithium niobate, intrinsic and extrinsic defects, density functional theory, molybdenum

(Some figures may appear in colour only in the online journal)

1. Introduction

Lithium niobate ($LiNbO_3$, LN) is one of the most used synthetic crystals as the compound presents fascinating photorefractive characteristics which make it possible for useful devices and platforms for integrated photonics [1–3]. As we know, the photorefractive properties of $LiNbO_3$ can be improved by doping with $Fe^{3+/2+}$, $Mn^{3+/2+}$, $Cu^{2+/+}$, or $Bi^{3+/2+}$ ions [4–9]. These materials are promising candidates for holographic storage applications. For example, bismuth (Bi) and magnesium (Mg) co-doped $LiNbO_3$ (LN:Bi,Mg) crystals can be used in the dynamic holographic display [5, 6]. While, molybdenum-doped $LiNbO_3$ (LN:Mo) is the only possible one for holographic storage from the ultraviolet to the visible with considerably shorter response time [10, 11]. However, there is still not enough accurate and detailed knowledge about LN defects in experiments. Due to the complicated structures of the LN crystals, it is difficult to trace the relationship between these different characteristics and different dopants directly by experimental techniques. The reason for the distinguished performance of LN:Mo is still unknown.

Recently, theoretical investigations play a more and more important role in the exploring the properties of crystals and explaining experimental phenomena. A number of theoretical simulations of the pure and doped $LiNbO_3$ have been carried out in the past few years [12–16]. In 2010, Xu *et al* explored

[1] Author to whom any correspondence should be addressed.

the site selection of $Fe^{2+/3+}$ ions [12], and Li *et al* revealed the relationship between the electronic states of Fe ions and the light absorption in the visible region [13]. In the case of bismuth-doped LN, the founding of special lone electron pair effect and small bound electron polaron are helpful in explaining the improved diffraction efficiency of Bi doped LN [14, 15]. However, there is no related report about molybdenum-doped $LiNbO_3$. The systematic analysis of the theoretical calculations on currently used dopants reveals that their charge states are all below +5, the valence of Nb, and the results show that these dopants preferably occupy the Li sites. Even in the vanadium-doped $LiNbO_3$, the V is found to prefer to substitute Li at its highest charge state of +5 [16]. It is known that the highest charge state of Mo is +6, which is higher than the charge state of Nb ions. Whether Mo-doped $LiNbO_3$ will occupy Nb sites or not is a tempting problem to be explored. And, the interaction between the Mo and intrinsic defects is another important characteristic that should be understood as the intrinsic defects Nb_{Li}^{4+} and V_{Li}^{-} are inevitable in LN crystals. The distribution of these point defects and the interaction between them are closely related to the properties of the crystal.

In addition, co-doping non-photorefractive ions with photorefractive ions could improve the laser-induced optical damage resistance and the response speed of $LiNbO_3$ crystals [17–19]. For example, the response time of Mo, Mg co-doped $LiNbO_3$ (LN:Mo,Mg) is dramatically shortened compared with LN:Mo [11]. The reason why Mo co-doped with non-photorefractive ions Mg, In and Zr perform better is hard to be figured out from the experiments. Therefore, theoretical calculations provide another way to understand the relationship between Mo and these non-photorefractive ions which will help us to select proper dopants and proper concentration in the crystal growth process.

In this work, based on the density functional theory (DFT), the defect formation energies, lattice distortions and electronic properties of LN:Mo point defects were explored [20, 21]. The site selection of Mo and its charge state are carried out based on the theoretical investigation and experimental study. In the present calculations, we intend to reveal the distributions and interactions between Mo and the intrinsic Nb_{Li}^{4+} and V_{Li}^{-} and extrinsic point defects. Furthermore, the density of states (DOS) and charge difference map of LN:Mo and LN:Mo,Mg are calculated to elucidate the effect of Mg ions on the electron distribution of LN:Mo,Mg crystal. Calculation details are collected in the method part.

2. Method

We used the Vienna *ab initio* simulation package (VASP) [22, 23] which performs an iterative solution of the Kohn–Sham equations with a plane-wave basis set. The energy cutoff for plane waves was 400 eV. The projector augmented wave (PAW) method was used to describe the electron–ion interactions. The Perdew–Burke–Ernzerh (PBE) function was adopted to treat the electron exchange and correlation energy [24, 25]. As we know that the PBE exchange–correlation functionals underestimate the band gap of perovskite materials, the hybrid exchange correlation functionals, such as B3LYP, B3PW and HSE06 allows to achieve an excellent agreement with the experiment for the band gaps of related ABO_3 perovskite materials [26, 27], however, the PBE functional can also describe the electronic properties accurately except the band gap. Here, the calculated band gap with PBE functional is about 3.37 eV; while the experiment result is usually 3.8 eV [28, 29], it is in the allowable error scope [30, 31]. Based on the PBE functional, one outer electron of Li ($2s^1$), six of O ($2s^2$, $2p^4$), eleven of Nb ($4p^6$, $4d^4$, $5s^1$), and six of Mo ($4d^5$, $5s^1$) were explicitly treated. Mo substituting Li (Mo_{Li}) and Mo substituting Nb site (Mo_{Nb}) point defects are calculated in the 240-atom hexagonal supercell. The same supercell is implemented in the situation that Mo_{Li} and Mo_{Nb} point defects coexist with intrinsic defects or extrinsic point defects Mg substituting Li site (Mg_{Li}), respectively. For $LiNbO_3$ hexagonal supercell, the length of the *c*-axis is more than twice the length of the *a* and *b* axis, thereby, a $4 \times 4 \times 2$ *k*-points mesh over the Brillouin zone with half number of *k* points in the *z* direction (*c* axis) as in *x* and *y* directions generated by the Monkhost–Pack scheme is employed [32]. As the supercell we employed is big enough, and to minimize the computational cost and save time, the Monkhost–Pack scheme used for defect pair calculation is a $2 \times 2 \times 1$ *k*-points mesh. For all the calculations, the structure is optimized with a force convergence criterion of 0.01 eV $Å^{-1}$.

Defect formation energy (DFE) as a criterion for judging the stability of point defects and defect clusters. The lower formation energy corresponds to the more stable defects [33]. The DFEs of Mo_{Li} and Mo_{Nb} point defects are calculated to explore the most stable charge state of the two point defects in LN:Mo. In order to find out the most suitable location distribution of Mo_{Li} and Mo_{Nb} point defects with intrinsic point defects lithium vacancy and Nb antisite, the DFEs of defect pairs are calculated, too. In general, DFE (E_F) can be calculated by [34, 35]

$$E_f(X^q) = E^{total}(X^q) - E^{total}(\text{perfect}) + \sum_i n_i\mu_i + q(E_F + E_v + \Delta V) \quad (1)$$

where *X* represents the point defect or the defect pairs and can be charged with *q* or electrically neutral. $E^{total}(X^q)$ is the total energy of the bulk with defect *X*, while E^{total}(perfect) is the total energy of the pristine supercell. *i* is the species of atoms that have been added to or removed from pristine crystal, n_i is the number of atoms *i*, and μ_i indicates the chemical potential of corresponding atoms *i*. $\Delta\mu_i$ is defined as differences from the bulk values of the chemical of atoms *i*. The chemical potential of Nb (μ_{Nb}), Li (μ_{Li}) and O (μ_O) atoms are calculated with DFT-PBE functional. They depend on the preparation conditions, and vary with the change of different reference phase in the constraints range. μ_{Nb}, μ_{Li} and μ_O should also satisfy with the formation of enthalpy of their oxides Li_2O and Nb_2O_5 [34, 36]

$$2\Delta\mu(Li) + \Delta\mu(O) = -\Delta H_f^{Li_2O} \quad (2)$$

Table 1. Chemical potentials of components in LN and doped LN by DFT-PBE under Li-rich and Li-deficient conditions.

Component	Chemical potential (eV)	
	Li-rich	Li-deficient
Li	−2.56	−3.63
Nb	−19.92	−18.96
O	−5.63	−5.59
Mo	−18.71	−18.83
Mg	−6.34	−6.30

$$2\Delta\mu\,(\mathrm{Nb}) + 5\Delta\mu\,(\mathrm{O}) = -\Delta H_{\mathrm{f}}^{\mathrm{Nb_2O_5}} \tag{3}$$

The relationship of μ_{Nb}, μ_{Li} and μ_{O} are also constrained by the equation of forming the stable $LiNbO_3$:

$$\Delta\mu(\mathrm{Li}) + \Delta\mu(\mathrm{Nb}) + 3\Delta\mu(\mathrm{O}) = -\Delta H_{\mathrm{f}}^{\mathrm{LiNbO_3}} \tag{4}$$

In addition, the restrictions of μ_{Mo}, is according to the experimental condition that Mo ions are from its oxide MoO_3, therefore, μ_{Mo} should satisfy with the requirement of forming the oxide MoO_3 [10]

$$\Delta\mu(\mathrm{Mo}) + 3\Delta\mu(\mathrm{O}) = -\Delta H_{\mathrm{f}}^{\mathrm{MoO_3}} \tag{5}$$

Similarly, the chemical potentials of extrinsic defects Mg ions μ_{Mg} is determined according to the formation enthalpy of their oxides,

$$\Delta\mu(\mathrm{Mg}) + \Delta\mu(\mathrm{O}) = -\Delta H_{\mathrm{f}}^{\mathrm{MgO}} \tag{6}$$

We have plotted the thermodynamically stable region of the LN in the former work to define the chemical potential of its components [37]. Table 1 lists the chemical potentials of Li, Nb, O, and Mo under Li-rich and Li-deficient conditions. As the as-grown crystals and films are Li-deficient composition, the chemical potentials of Nb and Li are employed according to the Li-deficient condition. The chemical potentials of Mo and Mg which are non-lithium niobate components are also calculated based on the chemical potential of O under the Li-deficient conditions. E_{v} is the valence band maximum (VBM) of crystals and E_{F} is the Fermi level in regard to the VBM. ΔV aligns with the reference potential difference between the defect supercell and the pristine crystal and it is related to the volume of the supercell. This term can be obtained from the electrostatic potentials difference between the region of defect and the region far from the defect [38]. The value of ΔV is 0.18 eV to the maximum in this calculation, and it brings a small impact when it plus with charge q.

As the total internal energies obtained from DFT calculations correspond to the Helmholtz free energy at zero temperature, there is a free energy correction between VASP work environment and real condition. The electronic entropy is negligible due to the large band gap of $LiNbO_3$, nonetheless, strain effects can be considered negligible in a large cell. The free energy ($F = E - TS$) is mainly related to the configuration contribution of point defects and defect clusters. At the room temperature of 300 K, the entropy of point defect and defect pair is about 0.16–0.20 eV [39–42].

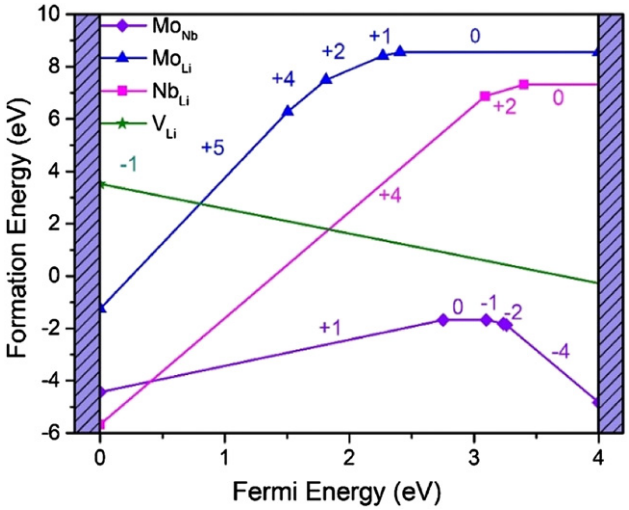

Figure 1. Defect formation energies of point defects Mo_{Li} and Mo_{Nb} with the most stable charge state, as well as the intrinsic defects Nb_{Li} and V_{Li} as a function of the Fermi energy. The Fermi energy range is from VBM to CBM.

Binding energy E_{b} as a criterion for judging the stability of a defect pair X_1X_2, usually be defined in terms of the formation energies [16, 34]

$$E_b\left[(X_1X_2)^q\right] = E_{\mathrm{f}}\left[(X_1X_2)^q\right] - E_{\mathrm{f}}\left[(X_1)^{q_1}\right] - E_{\mathrm{f}}\left[(X_2)^{q_2}\right] \tag{7}$$

where $q = q_1 + q_2$, the negative binding energy means that the energy required to separate the defect pair into two individual defects X_1 and X_2 is more than the formation energy of defect pair X_1X_2, which indicates a stable defect pair.

3. Results and discussion

3.1. Point defects in the LN:Mo crystal

In this study, we first calculate the formation energies of Mo substituting Li (Mo_{Li}) and Nb (Mo_{Nb}) at all possible charge states in a 240-atom supercell based on the DFT-PBE. The results are shown in figure 1. It can be seen that Mo prefers to occupy the Li site at the +6 charge state when the Fermi energy is close to the VBM. With the increase of Fermi energy which is mainly due to the increase of dopants concentration, the Mo_{Li}^{5+} transfers to Mo_{Li}^{4+} when the Fermi energy E_{F} = 1.50 eV. At this time, the charge state of Mo and Nb are the same, and then Mo_{Li}^{4+} transfers to Mo_{Li}^{2+} directly by capturing two electrons, it seems like the transition behavior of Nb_{Li}. Mo_{Li}^{+} presents as the most stable charge state in a short range of Fermi energy from 1.95 eV to 2.08 eV. The results indicate that Mo_{Li}^{3+} is metastable, due to the negative U effect [43], the thermodynamic transition level $\varepsilon(+4/+3)$ is higher than $\varepsilon(+3/+2)$, therefore, the Mo_{Li}^{3+} cannot be shown as a stable charge state in figure 1. While in the most $LiNbO_3$ crystals, the Fermi level lies in the lower half of the band gap, therefore, Mo_{Li}^{5+}, Mo_{Li}^{4+}, and Mo_{Li}^{2+} are stable point defects of Mo in Li sites. Compared with the results of Nb_{Li} point defect, we found that Mo_{Li} possesses a higher formation

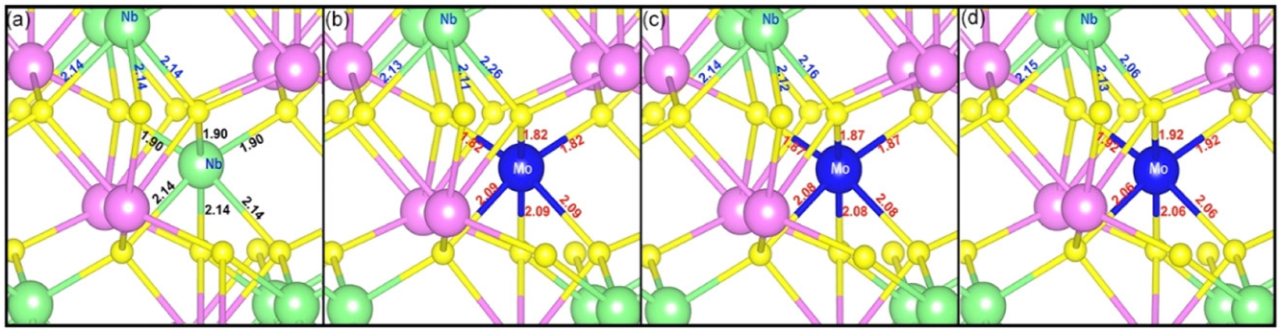

Figure 2. The local lattice of distortion of (a) pristine and (b) Mo^{+}_{Nb}, (c) Mo^{0}_{Nb}, (d) Mo^{-}_{Nb} point defects. The number labeled on the bond is the distance between the defects and its neighboring O ions (the black and red numbers), and the distance between the normal Nb site and its neighboring O ions (the blue numbers). The unit of these numbers is Å.

energy in the whole Fermi energy range. It is difficult for Mo ions to push the Nb-antisite to the normal position like other dopants.

In the case of Mo_{Nb}, Mo^{6+} is the most stable charge state in the most possible Fermi energy range, then Mo^{6+} will transfer to Mo^{5+} which presents the same charge state as Nb ions. Mo^{5+} as the most stable state is maintained within the Fermi range 2.75–3.10 eV. Mo substituting Nb ions with +4 and +3 charge state also appears in a short Fermi range. When the Fermi energy close to the conduction band minimum (CBM), the most stable charge state of Mo_{Nb} is −4. The same as Mo occupies the Li site, the lowest charge state of Mo ions at Nb site occurs near the CBM, which indicates a high concentration of dopants. In the entire Fermi energy range, Mo_{Nb} possesses lower formation energy than Mo_{Li}, which illustrates that Mo ions prefer to substitute Nb ions forming Mo^{+}_{Nb} point defect.

The results are different from other doped $LiNbO_3$ that have been reported. In the most doped $LiNbO_3$, the ions sit on the Li site with its highest charge state show the lowest formation energies [12–16]. However, the Mo ions tend to occupy the Nb site with its highest charge state +6. Single crystal x-ray diffraction experiment results also confirmed that Mo occupies the niobium site in the crystals [10]. As the fact that in the most $LiNbO_3$ crystals, the Fermi level lies in the lower half of the band gap, Mo ions with higher charge state +4, +5, +6 are more reasonable. The experiment results of x-ray photoelectron spectroscopy (XPS) imply the coexistence of Mo^{6+}, Mo^{5+}, and Mo^{4+} [10].

Here, the formation energy of intrinsic Nb antisite and Li vacancy defects are drawn for comparison. The formation energy and stable chsrge state of Nb_{Li} and V_{Li} show similar change with the results that have been reported [14, 16, 35]. Based on the results above, we compare the formation energy of Mo_{Nb} with the stable intrinsic Nb^{4+}_{Li} and V^{-}_{Li} defects, found the formation energy of Mo_{Nb} is much lower than that of V_{Li} in the possible Fermi range. And Mo_{Nb} is easier to form beyond $E_F = 0.4$ eV compared with Nb_{Li}, while Nb_{Li} is easier below $E_F = 0.4$ eV. The results indicate that Mo_{Nb} and Nb^{4+}_{Li} can coexist in the crystals, therefore, Mo^{+}_{Nb} is formed easily in both stoichiometric and congruent $LiNbO_3$ crystals. We will discuss the interaction between them later.

In order to understand the influence that Mo substituting Nb site brings to the bulk, we investigate the localized structural relaxations of the most stable Mo^{+}_{Nb}, Mo^{0}_{Nb} and Mo^{-}_{Nb} point defects in figure 2. For Mo^{+}_{Nb}, as shown in figures 2(a) and (b), we can see that the Mo–O_{upper} bond length decreases to 1.82 Å compared with the pristine Nb–O bond length 1.90 Å, the Mo–O_{lower} bond length also decreases by about 2.3%. There is a significant shrinkage of the oxygen octahedron around the Mo_{Nb} defect. While in the case of normal Nb site, it can be seen that the distances between Nb and two lower neighboring O site are also a little decrease. However, the O ion that is simultaneously bonded to the normal Nb and Mo ion become an exception, the bond length between the O ion and normal Nb ion increases. The reason for this phenomenon is the stronger covalent bond of Mo–O as compared to Nb–O. And it may lead to a deformation in electron cloud of the oxygen ions, which is related to the narrower band gap. This corresponds to the red shift of the absorption edge of the LN:Mo crystals in contrast to CLN [10]. And we can see the similar shrinkage of the oxygen octahedron around the Mo_{Nb} defect in the situation of Mo^{0}_{Nb} and Mo^{-}_{Nb} point defects. While the severity of shrinkage decreases with the decreasing charge state of Mo ions due to the stronger Coulomb repulsion between the trapped electrons and electrons around O ions.

The discussion about the lattice distortion of point defects lays the foundation for the study of whether Mo can become a photorefractive center or not. As we mentioned above, the transition between Mo^{4+}_{Li} and Mo^{2+}_{Li} is similar to the situation of Nb^{4+}_{Li} and Nb^{2+}_{Li}. If Nb^{4+}_{Li} capture two electrons to form Nb^{2+}_{Li}, and introduce the lattice distortion between Nb^{2+}_{Li} and its neighbor normal Nb site, then Nb^{2+}_{Li} can be treated as a $4d^1$–$4d^1$ bipolaron [44]. In figure 3(a), we show the charge density difference map of Mo^{4+}_{Li} and Mo^{2+}_{Li}. It can be seen that the two captured electrons are distributed around the Mo^{2+}_{Li} and its neighboring Nb. The results are in contrast to the situation of Nb^{2+}_{Li}, therefore, Mo^{2+}_{Li} can also be treated as a $4d^1$–$4d^1$ bipolaron, which means that $Mo^{2+/4+}_{Li}$ serves as a photorefractive center in the crystals. Whether Mo substituting Nb site can also be the photorefractive center is a problem to be discussed. If Mo^{+}_{Nb} capture two electrons then it can be treated as the Mo^{-}_{Nb}, another stable charge state in Mo point defect. In figure 3(b), the charge density difference map of Mo^{+}_{Nb} and

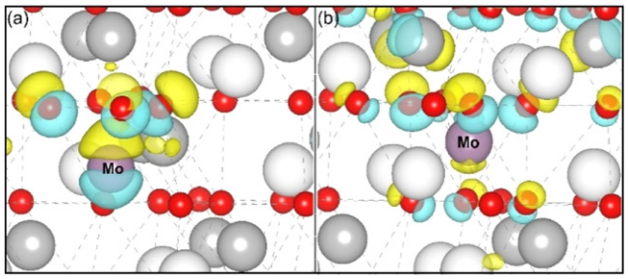

Figure 3. The charge density difference map of (a) Mo_{Li}^{4+} and Mo_{Li}^{2+}, (b) Mo_{Nb}^{+} and Mo_{Nb}^{-}. The white, gray, red and blue balls denote the Li, Nb, O and Mo atoms respectively.

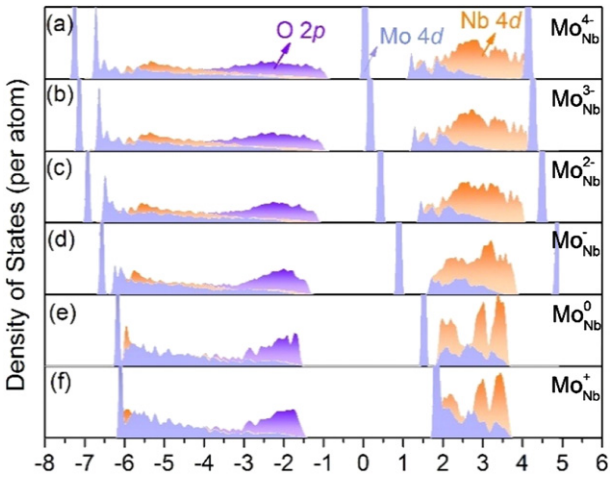

Figure 4. PDOS of the Mo_{Nb} point defect with charge state from −4 to +1 (a)–(f). The contribution of $LiNbO_3$ elements are shown with different colors. The contribution of Mo_{Nb} is labeled as light blue.

Mo_{Nb}^{-} is plotted. Seen from it, the trapped electrons are found also mainly gathered around Mo_{Nb}^{-} as Mo_{Li}^{2+} which leads to the lattice distortion we discussed above. Similar results illustrate that Mo_{Nb} may also be a photorefractive center. In LN:Mo, both Mo_{Li} and Mo_{Nb} are contributors to the photorefraction effect.

Differently from the dopants such as vanadium and bismuth, Mo substituting Nb position may present a positive charge state. To explore the particularity of Mo_{Nb}, we draw the partial density of states (PDOS) of Mo_{Nb} point defects with different charge states in figure 4. Seen from it, there is a density of states peaks which are made up of Mo-4d electrons in the middle of the band gap of LN:Mo with Mo_{Nb} point defects. It illustrates that Mo_{Nb} forms new energy levels in the band gap. With Mo ion losing electrons, the energy level of Mo gradually approaches to CBM, and when all the six outer electrons of Mo are lost, the contribution of Mo_{Nb} overlap to the contribution of Nb elements. The plentiful energy levels facilitate the electronic transitions between different energy levels, which corresponding to the experiment results that there are absorption peaks in the visible range [10, 11]. Therefore, Mo-doped $LiNbO_3$ indeed improves the photorefractive effect of crystals in the all visible light range.

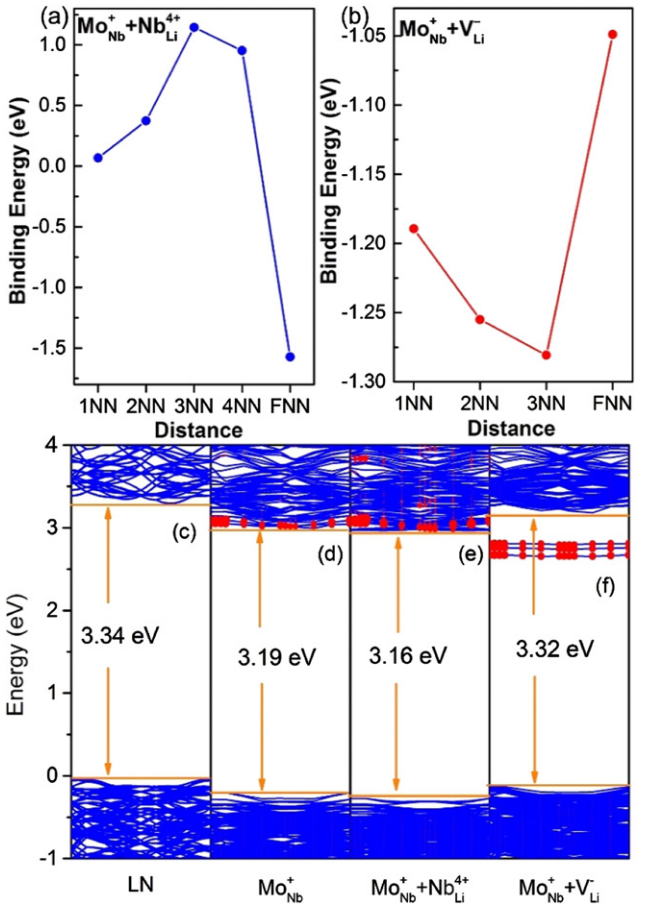

Figure 5. The binding energy of Mo_{Nb}^{+} defect with intrinsic defect (a) Nb_{Li}^{4+} and (b) V_{Li}^{-} with different distances. 1NN to 4NN are corresponding to the position of Nb_{Li}^{4+} or V_{Li}^{-} which lie in the first to the forth nearest neighboring sites of Mo_{Nb}^{+}, and the FNN is a site far away from the Mo_{Nb}^{+} site. (c)–(f) show the band structures of LN pristine and LN with Mo_{Nb}^{+}, Mo_{Nb}^{+} + Nb_{Li}^{4+}, and Mo_{Nb}^{+} + V_{Li}^{-} defects. The red lines are the energy levels of Mo ions.

3.2. Mo point defect with intrinsic point defect

From the analysis of the defect formation energies of Mo_{Nb} point defect as well as the intrinsic defects Nb_{Li}^{4+} and V_{Li}^{-}, we believe that Mo_{Nb}^{+}, Nb_{Li}^{4+} and V_{Li}^{-} coexist in the $LiNbO_3$ crystal. Based on the results above, the distribution of Mo_{Nb}^{+} and Nb_{Li}^{4+} defects is explored in figure 5(a). As both of the two point defects present the positive charge state, the distance between them would be enlarged due to the obvious Coulombic repulsion when they are close to each other. The binding energy of the Mo_{Nb}^{+} and Nb_{Li}^{4+} defect pair increases with the distance increased from the first nearest neighbor (1NN) to the third nearest neighbor (3NN), then it decreases to −1.5 eV until the Nb_{Li}^{4+} is far away from the Mo_{Nb}^{+}. The binding energies of Mo_{Nb}^{+} and Nb_{Li}^{4+} defect pair are found to be positive except when they separate from each other, therefore, it is suitable to separate Mo_{Nb}^{+} and Nb_{Li}^{4+} to single defects. While as Mo substitute Nb site, the extra Nb may lead to more Nb_{Li}^{4+} antisite. On the one hand, the additional Nb_{Li}^{4+} defects can also play the role of the photorefractive center; on the other hand, to maintain an electrically neutral environment in the

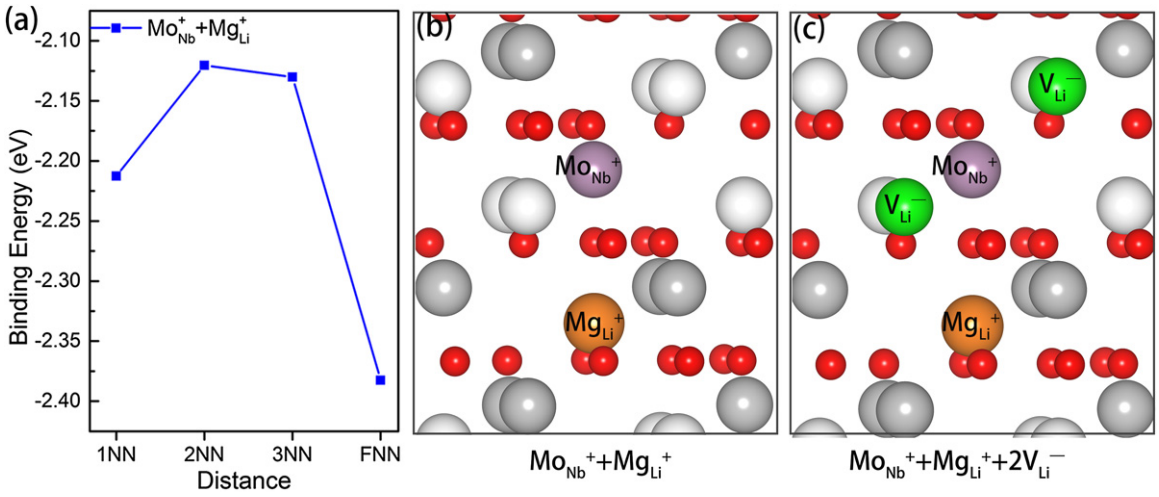

Figure 6. (a) The binding energy of Mo_{Nb}^{+} defect with extrinsic defect Mg_{Li}^{+}, 1NN to 3NN are corresponding to the position of Mg_{Li}^{+} which lie in the first to the third nearest neighboring sites of Mo_{Nb}^{+}, FNN is a site far away from Mo_{Nb}^{+} site. (b) The structure of $Mg_{Li}^{+}+Mo_{Nb}^{+}$ defect pair, (c) the distribution of V_{Li}^{-} in the $Mg_{Li}^{+}+Mo_{Nb}^{+}+2V_{Li}^{-}$ cluster.

crystal, more lithium vacancies are required for charge compensation. The distribution of Mo_{Nb}^{+} and V_{Li}^{-} is also explored in figure 5(b).

The binding energy of Mo_{Nb}^{+} and V_{Li}^{-} defect pair shows the lowest formation energy when V_{Li}^{-} is the third nearest neighbor of Mo_{Nb}^{+}. The highest binding energy happened in the situation that V_{Li}^{-} is far away from Mo_{Nb}^{+}. The results are different from the case of $Mo_{Nb}^{+}+Nb_{Li}^{4+}$ defect pair. It illustrates that $Mo_{Nb}^{+}+V_{Li}^{-}$ is a stable defect pair when they as the 3NN of each other. As we know that V_{Li}^{-} will affect the oxygen ions around it, by the way of V_{Li}^{-}, Mo_{Nb}^{+} may introduce the effect on the distribution of electrons around them.

In figures 5(c)–(f), we show the band structures of $LiNbO_3$ bulk, Mo_{Nb}^{+} point defect, $Mo_{Nb}^{+}+Nb_{Li}^{4+}$ and $Mo_{Nb}^{+}+V_{Li}^{-}$ defect pairs. We can see a narrower band gap with Mo ions added to the LN system. This is in line with our previous conclusion that the Mo–O bond is more stable than the Nb–O bond which may lead to the red shift of the absorption edge. Seen from figure 5(d), there is no obvious energy level in the band gap, the contribution of Mo ions distributed in the conduction band, and they overlap with the conduction band. It indicates that Mo ions can make an extra absorption in the ultraviolet region when the electrons transit from the valence band to the Mo energy level. The results are matching with the experiments that there is an absorption peak at 337 nm. The band structure of $Mo_{Nb}^{+}+Nb_{Li}^{4+}$ defect pair is shown in figure 5(e). There are no significant differences between the Mo_{Nb}^{+} point defect and $Mo_{Nb}^{+}+Nb_{Li}^{4+}$ defect pair. This performance also provides proof that Mo_{Nb}^{+} and Nb_{Li}^{4+} have no interaction with each other, which indicate that Mo_{Nb}^{+} and Nb_{Li}^{4+} should be separated from each other. In the band structure of $Mo_{Nb}^{+}+V_{Li}^{-}$ defect pair, there are some new energy levels in the band gap, which are about 0.4 eV away from the bottom of the conduction band. These defect levels provide an opportunity of electron transition from defect levels to conduction band. It may correspond to the absorption peak in the visible light region.

Table 2. The formation energies of different lithium vacancies distributions around $Mg_{Li}^{+}+Mo_{Nb}^{+}$ defect pair with a reference of Mo_{Nb}^{+}.

Distribution of the two lithium vacancies	Formation energies (eV)
2NN + 2NN	1.42
3NN + 3NN	1.49
2NN + 3NN	1.37

3.3. Mo point defect with extrinsic point defect

In this section, we investigated the properties of LN:Mo,Mg. Learning from the result of Li *et al*, Mg ions prefer the Li site in the LN crystals [13]. Therefore, when Mo co-doped with Mg ions, Mo ions will occupy Nb ions while Mg ions will substitute Li site. The distribution of the Mo ions with Mg ions in different distance is discussed in figure 6, respectively. Mg_{Li}^{+} as the first, second, third and faraway nearest neighbors of Mo_{Nb}^{+} point defect are considered, respectively. Seen from figure 6, as the function of the Coulombic repulsion between two positive point defects, when Mg_{Li}^{+} is far away from Mo_{Nb}^{+}, the defect pairs show the lowest binding energy. In figure 6(a), the negative binding energies illustrate that it is easy to form a defect pair of $Mg_{Li}^{+}+Mo_{Nb}^{+}$. To maintain the neutral environment in the crystal, the $Mg_{Li}^{+}+Mo_{Nb}^{+}$ defect pair should be charge compensated by the intrinsic defect V_{Li}^{-} to form a stable defect cluster. However, if Mg_{Li}^{+} is faraway from the Mo_{Nb}^{+} point defect, the interaction between them is too weak to be explored. Therefore, Mg_{Li}^{+} as the first nearest neighbor

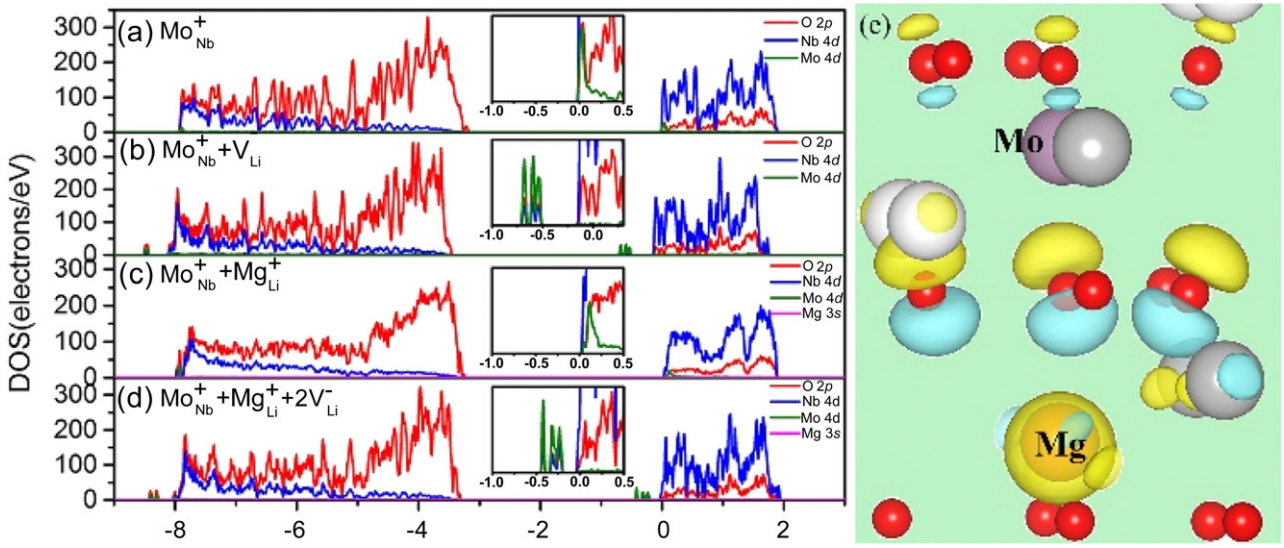

Figure 7. The density of states of (a) Mo^{+}_{Nb} point defect, (b) $Mo^{+}_{Nb} + V^{-}_{Li}$ defect pair, (c) $Mg^{+}_{Li} + Mo^{+}_{Nb}$ defect pair, and (d) $Mg^{+}_{Li} + Mo^{+}_{Nb} + 2V^{-}_{Li}$ defect cluster. The magnified area shows that the influence of Mo atoms. (e) Electronic charge difference map between $Mg^{+}_{Li} + Mo^{+}_{Nb}$ and Mo^{+}_{Nb}. Yellow and blue ellipsoid represent electron depletion and accumulation, respectively. The white, gray, red, orange and purple balls denote the Li, Nb, O, Mg and Mo atoms, respectively.

is also taken into consideration in the process of clustering. Figure 6(b) shows the structure of $Mg^{+}_{Li} + Mo^{+}_{Nb}$ defect pair, the distribution of V^{-}_{Li} are discussed in the following.

According to the results in table 2, in the possible configerations of $Mg^{+}_{Li} + Mo^{+}_{Nb} + 2V^{-}_{Li}$ cluster, the structure that one of the lithium vacancies is the second nearest neighbor of Mo^{+}_{Nb} while the other one is the third nearest neighbor of Mo^{+}_{Nb} is most stable. In this structure, one lithium vacancy is upper the defect pair $Mg^{+}_{Li} + Mo^{+}_{Nb}$, the other is in the defect pair as shown in figure 6(c). The result is consistent with the above conclusion that V^{-}_{Li} prefers to be the 3NN of Mo^{+}_{Nb}. In order to explore the relationship between Mo^{+}_{Nb} and Mg^{+}_{Li}, we draw the PDOS of $Mg^{+}_{Li} + Mo^{+}_{Nb}$ defect pair, and Mo^{+}_{Nb} point defect, $Mo^{+}_{Nb} + V^{-}_{Li}$ defect pair, and $Mg^{+}_{Li} + Mo^{+}_{Nb} + 2V^{-}_{Li}$ defect cluster for comparison. From the PDOS of Mo^{+}_{Nb} in figure 7(a), it can be seen that the contribution of Mo 4d overlaps with the states of Nb 4d. From the band structure in figures 5(e) and (f), under the influence of V^{-}_{Li}, the energy levels of Mo are separated from the conduction band. The same conclusion can also be obtained from figure 7(b). While the combination with Mg^{+}_{Li} point defect does not change the distribution of Mo 4d features, the d electrons of Mo and Nb still overlap together. When the $Mg^{+}_{Li} + Mo^{+}_{Nb}$ defect pair forms the stable defect cluster with V^{-}_{Li}, the states of Mo 4d separate from the conduction band too, however, the Mo 4d electrons are a little closer to the conduction band compared to the situation of $Mo^{+}_{Nb} + V^{-}_{Li}$ defect pair. The properties of Mo^{+}_{Nb} have changed under the combined action of Mg^{+}_{Li} and V^{-}_{Li}. To seek for the effect of Mg ions, the electronic charge difference map between the $Mg^{+}_{Li} + Mo^{+}_{Nb}$ defect pair and Mo^{+}_{Nb} point defect is given in figure 7(e). There is a significant loss of electronics around the Mg ion. And the distribution of electrons of the O atoms that around the Mg ion also change a lot. It illustrates that the oxygen atoms are more active which will help with the decrease of response time [5, 45]. Therefore, Mo and Mg co-doped $LiNbO_3$ possess more superior photorefractive properties compared with Mo doped $LiNbO_3$.

4. Conclusion

In summary, we have performed the detailed first-principles calculations of the possible site preference in isolate defects and corresponding charge state in LN:Mo. Mo substituting Nb with its highest charge state +6 is found to be the most stable point defect form. Both Mo_{Li} and Mo_{Nb} are photorefractive centers which improve its photorefractive performance in $LiNbO_3$ crystals. The distribution of defect energies from VBM to CBM formed by Mo ions with different charge states is in line with the absorption in the visible region. While the energy levels of Mo^{+}_{Nb} in the conduction band are responsible for the absorption in the ultraviolet region. Also, Mo^{+}_{Nb} and Nb^{4+}_{Li} point defects should be separated from each other, and they show a weak influence on each other. While the $Mo^{+}_{Nb} + V^{-}_{Li}$ defect pair is stable when Mo^{+}_{Nb} and V^{-}_{Li} are the third nearest neighbors of each other, and the V^{-}_{Li} could cause the movement of the Mo^{+}_{Nb} energy levels. In addition, the combination with Mg^{+}_{Li} point defect do not shift the energy level of Mo, and Mg ions have an influence on the distribution of electrons of LN:Mo,Mg, then the photorefractive properties are improved.

Conflict of interest

There are no conflicts to declare.

Acknowledgments

We gratefully acknowledge financial support from National Natural Science Foundation of China with Grant Number

[11674179] and [61705116], and the Program for Changjiang Scholars and the Innovative Research Team in University with Grant Number [IRT_13R29].

ORCID iDs

Hongde Liu https://orcid.org/0000-0003-2183-9609
Lixin Zhang https://orcid.org/0000-0002-3289-2272

References

[1] Zhang M, Wang C, Cheng R, Shams-Ansari A and Lončar M 2017 Monolithic ultra-high-Q lithium niobate microring resonator *Optica* **4** 1536
[2] Guarino A, Poberaj G, Rezzonico D, Degl'Innocenti R and Guenter P 2007 Electro-optically tunable microring resonators in lithium niobate *Nat. Photon.* **1** 407
[3] Arizmendi L 2004 Photonic applications of lithium niobate crystals *Phys. Status Solidi* A **201** 253
[4] Buse K, Adibi A and Psaltis D 1998 Non-volatile holographic storage in doubly doped lithium niobate crystals *Nature* **393** 665
[5] Zheng D, Kong Y, Liu S, Yao J, Zhang L, Chen S and Xu J 2015 The photorefractive characteristics of bismuth-oxide doped lithium niobate crystals *AIP Adv.* **5** 017132
[6] Zheng D, Kong Y, Liu S, Chen M, Chen S, Zhang L, Rupp R and Xu J 2016 The simultaneous enhancement of photorefraction and optical damage resistance in MgO and Bi_2O_3 co-doped $LiNbO_3$ crystals *Sci. Rep.* **6** 20308
[7] Guo Y, Liao Y, Cao L, Liu G, He Q and Jin G 2004 Improvement of photorefractive properties and holographic applications of lithium niobate crystal *Opt. Express* **12** 5556
[8] Phillips W, Amodei J J and Staebler D L 1972 Optical and holographic storage properties of transition metal doped lithium niobate *RCA Rev.* **33** 94
[9] McMillen D K, Hudson T D, Wagner J and Singleton J 1998 Holographic recording in specially doped lithium niobate crystals *Opt. Express* **2** 491
[10] Tian T, Kong Y, Liu S, Li W, Wu L, Chen S and Xu J 2012 Photorefraction of molybdenum-doped lithium niobate crystals *Opt. Lett.* **37** 2679
[11] Tian T, Kong Y, Liu S, Li W, Chen S, Rupp R and Xu J 2013 Fast UV-vis photorefractive response of Zr and Mg codoped $LiNbO_3$:Mo *Opt. Express* **21** 10460
[12] Xu H, Chernatynskiy A, Lee D, He J, Sinnott S B, Gopalan V, Dierolf V and Phillpot S R 2010 Stability and charge transfer levels of extrinsic defects in $LiNbO_3$ *Phys. Rev.* B **82** 184109
[13] Li L, Li Y and Zhao X 2018 Doping stability of nonphotorefractive ions in stoichiometric and congruent $LiNbO_3$ *Phys. Chem. Chem. Phys.* **20** 17477
[14] Li Y, Li L and Zhao X 2017 Hybrid density functional theory insight into the stability and microscopic properties of Bi-doped $LiNbO_3$: lone electron pair effect *Phys. Rev.* B **96** 115118
[15] Li L, Li Y and Zhao X 2019 Interaction between Bi dopants and intrinsic defects in $LiNbO_3$ from local and hybrid density functional theory calculations *Inorg. Chem.* **58** 3661
[16] Fan Y, Li L, Li Y, Sun X and Zhao X 2019 Hybrid density functional theory study of vanadium doping in stoichiometric and congruent $LiNbO_3$ *Phys. Rev.* B **99** 035147
[17] Zhang G, Xu J, Liu S, Sun Q, Zhang G, Fang Q and Ma C 1995 Study of resistance against photorefractive light-induced scattering in $LiNbO_3$:Fe,Mg crystals *Proc. SPIE* **2529** 14
[18] Kong Y, Wu S, Liu S, Chen S and Xu J 2008 Fast photorefractive response and high sensitivity of Zr and Fe co-doped $LiNbO_3$ crystals *Appl. Phys. Lett.* **92** 251107
[19] Zhu L, Zheng D, Liu H, Saeed S, Wang S, Liu S, Chen S, Kong Y and Xu J 2018 Enhanced photorefractive properties of indium co-doped $LiNbO_3$:Mo crystals *AIP Adv.* **8** 095316
[20] Hohenberg P and Kohn W 1964 Inhomogeneous electron gas *Phys. Rev.* **136** B864
[21] Kohn W and Sham L J 1965 Self-consistent equations including exchange and correlation effects *Phys. Rev.* **140** A1133
[22] Kresse G and Furthmüller J 1996 Efficiency of ab initio total energy calculations for metals and semiconductors using a plane-wave basis set *Comput. Mater. Sci.* **6** 15
[23] Kresse G and Furthmüller J 1996 Efficient iterative schemes for ab initio total-energy calculations using a plane wave basis set *Phys. Rev.* B **54** 11169
[24] Kresse G and Joubert D 1999 From ultrasoft pseudopotentials to the projector augmented-wave method *Phys. Rev.* B **59** 1758
[25] Perdew J P, Burke K and Ernzerhof M 1996 Generalized gradient approximation made simple *Phys. Rev. Lett.* **77** 3865
[26] Eglitis R I and Popov A I 2018 Systematic trends in (001) surface ab initio calculations of ABO_3 perovskites *J. Saudi Chem. Soc.* **22** 459
[27] Eglitis R I 2013 Ab initio calculations of the atomic and electronic structure of $BaZrO_3$ (111) surfaces *Solid State Ion.* **230** 43
[28] Redfield D and Burke W J 1974 Optical absorption edge of $LiNbO_3$ *J. Appl. Phys.* **45** 4566
[29] Dhar A and Mansingh A 1990 Optical properties of reduced lithium niobate single crystals *J. Appl. Phys.* **68** 5804
[30] Hybertsen M S and Louie S G 1985 First-principles theory of quasiparticles: calculation of band gaps in semiconductors and insulators *Phys. Rev. Lett.* **55** 1418
[31] Godby R W, Schlüter M and Sham L J 1988 Self-energy operators and exchange-correlation potentials in semiconductors *Phys. Rev.* B **37** 10159
[32] Monkhorst H J and Pack J D 1976 Special points for Brillonln-zone integrations *Phys. Rev.* B **13** 5188
[33] Xu H, Lee D, Sinnott S B, Gopalan V, Dierolf V and Phillpot S R 2009 Structure and energetics of Er defects in $LiNbO_3$ from first-principles and thermodynamic calculations *Phys. Rev.* B **80** 144104
[34] Van de Walle C G and Neugebauer J 2004 First-principles calculations for defects and impurities: applications to III-nitrides *J. Appl. Phys.* **95** 3851
[35] Lany S and Zunger A 2008 Assessment of correction methods for the band-gap problem and for finite-size effects in supercell defect calculations: case studies for ZnO and GaAs *Phys. Rev.* B **78** 235104
[36] Xu H, Lee D, He J, Sinnott S B, Gopalan V, Dierolf V and Phillpot S R 2008 Stability of intrinsic defects and defect clusters in $LiNbO_3$ from density functional theory calculations *Phys. Rev.* B **78** 174103
[37] Wang W, Zheng D, Hu M, Saeed S, Liu H, Kong Y, Zhang L and Xu J 2019 Effect of defects on spontaneous polarization in pure and doped $LiNbO_3$: first-principles calculations *Materials* **12** 100
[38] Komsa H P, Rantala T T and Pasquarello A 2012 Finite-size supercell correction schemes for charged defect calculations *Phys. Rev.* B **86** 045112
[39] Li Y, Schmidt W G and Sanna S 2015 Defect complexes in congruent $LiNbO_3$ and their optical signatures *Phys. Rev.* B **91** 174106
[40] Kohan A F, Ceder G, Morgan D and Van de Walle C G 2000 First-principles study of native point defects in ZnO *Phys. Rev.* B **61** 15019
[41] He J, Behera R K, Finnis M W, Li X, Dickey E C, Phillpot S R and Sinnott S B 2007 Prediction of high-temperature

point defect formation in TiO_2 from combined ab initio and thermodynamic calculations *Acta Mater.* **55** 4325

[42] Wang W, Zhong Y, Zheng D, Liu H, Kong Y, Zhang L, Rupp R and Xu J 2020 p-type conductivity mechanism and defect structure of N doped $LiNbO_3$ from first-principles calculations *Phys. Chem. Chem. Phys.* **22** 20

[43] Anderson P W 1975 Model for the electronic structure of amorphous semiconductors *Phys. Rev. Lett.* **34** 953

[44] Nahm H H and Park C H 2008 First-principles study of microscopic properties of the Nb antisite in $LiNbO_3$: comparison to phenomenological polaron theory *Phys. Rev.* B **78** 184108

[45] Zheng D, Wang W, Wang S, Qu D, Liu H, Kong Y, Chen S, Rupp R and Xu J 2019 Real-time dynamic holographic display realized by bismuth and magnesium co-doped lithium niobate *Appl. Phys. Lett.* **114** 241903